1 **Title:** PREDICTION OF PRIMARY SOMATOSENSORY NEURON ACTIVITY

2 DURING ACTIVE TACTILE EXPLORATION

3 **Authors:** Dario Campagner[1], Mathew Evans[1], Michael R. Bale[1,2], Andrew Erskine[1,3],

4 Rasmus S. Petersen[1]

5 **Authors' affiliation:** 1. Faculty of Life Sciences, University of Manchester, Stopford

6 Building, Oxford Road, Manchester M13 9PT, UK. 2. School of Life Sciences, University of

7 Sussex, Brighton, BN1 9QG, UK 3. The Francis Crick Institute, Mill Hill Laboratory, The

8 Ridgeway, Mill Hill, London, NW7 1AA.

9 **Correspondence to:** r.petersen@manchester.ac.uk

10

11

ABSTRACT

Primary sensory neurons form the interface between world and brain. Their function is well-understood during passive stimulation but, under natural behaving conditions, sense organs are under active, motor control. In an attempt to predict primary neuron firing under natural conditions of sensorimotor integration, we recorded from primary mechanosensory neurons of awake, head-fixed mice as they explored a pole with their whiskers, and simultaneously measured both whisker motion and forces with high-speed videography. Using Generalised Linear Models, we found that primary neuron responses were poorly predicted by whisker angle, but well-predicted by rotational forces acting on the whisker: both during touch and free-air whisker motion. These results are in apparent contrast to previous studies of passive stimulation, but could be reconciled by differences in the kinematics-force relationship between active and passive conditions. Thus, simple statistical models can predict rich neural activity elicited by natural, exploratory behaviour involving active movement of the sense organs.

INTRODUCTION

A major challenge of sensory neuroscience is to understand the encoding properties of neurons to the point that their spiking activity can be predicted in the awake animal, during natural behaviour. However, accurate prediction is difficult without experimental control of stimulus parameters and, despite early studies of awake, behaving animals (Hubel, 1959), subsequent work has most often effected experimental control by employing anaesthesia and/or passive stimulation. However, the active character of sensation (Gibson, 1962; Yarbus 1967), based on motor control of the sense organs, is lost in reduced preparations. Recent methodological advances permit a way forward: in the whisker system, it is now possible to record neuronal activity from an awake mouse, actively exploring the environment with its whiskers, whilst simultaneously measuring the fundamental sensory variables (whisker kinematics and mechanics) likely to influence neuronal activity (O'Connor et al. 2010).

Our aim here was to predict spikes fired by primary whisker neurons (PWNs) of awake mice engaged in natural, object exploration behaviour. The manner in which primary neurons encode sensory information fundamentally constrains all downstream neural processing (Lettvin et al. 1959). PWNs innervate mechanoreceptors located in the whisker follicles (Zucker and Welker 1969; Rice et al. 1986). They are both functionally and morphologically diverse; including types responsive to whisker-object contact and/or whisker self-motion (Szwed et al. 2003; Ebara et al. 2002). PWNs project to the cerebral cortex, analogously to other modalities, via trisynaptic pathways through the brainstem and thalamus (Diamond et al. 2008).

Here, we show that PWN responses are well-predicted by rotational force ('moment') acting on the whisker, while whisker angle is a poor predictor. Moment coding accounts for a substantial amount of spiking during both whisker-object interaction and whisker motion in

3

52   air. Moment coding can also account for findings in previous studies of passive stimulation in

53   the anaesthetized animal; indicating that the same biomechanical framework can account for

54   primary somatosensory neurons responses across diverse states. Our results provide a

55   mechanical basis for linking receptor mechanisms to tactile behaviour.

56   **RESULTS:**

57   **Primary whisker neuron activity during object exploration is predicted by whisker**

58   **bending moment**

59   We recorded the activity of single PWNs from awake mice (Figure 1A, E, Figure 1-figure

60   supplement 1) as they actively explored a metal pole with their whiskers (N = 20 units). At

61   the same time, we recorded whisker motion and whisker shape using high-speed videography

62   (1000 frames/s; Figure1D, Video 1). As detailed below, PWNs were diverse, with some

63   responding only to touch, others also to whisker motion. Since each PWN innervates a single

64   whisker follicle, we tracked the 'principal whisker' of each recorded unit from frame to

65   frame, and extracted both the angle and curvature of the principal whisker in each video

66   frame (total 1,496,033 frames; Figure1B-E; Bale et al. 2015). Whiskers are intrinsically

67   curved, and the bending moment on a whisker is proportional to how much this curvature

68   changes due to object contact (Birdwell et al. 2007): we therefore used 'curvature change' as

69   a proxy for bending moment (O'Connor et al. 2010a). Whisker-pole contacts caused

70   substantial whisker bending (curvature change), partially correlated with the whisker angle

71   (Figures 1E, 4E) and, consistent with Szwed et al. (2003) and Leiser and Moxon (2007),

72   robust spiking (Figures 1E, 2E).

73   To test between candidate encoding variables, our strategy was to determine how accurately

74   it was possible to predict PWN activity from either the angular position or curvature change

75   of each recorded unit's principal whisker. To predict spikes from whisker state, we used

4

76   Generalised Linear Models (GLMs; Figure 2A). GLMs, driven by whisker angle, have

77   previously been shown to provide a simple but accurate description of the response of PWNs

78   to passive stimulation (Bale et al. 2013) and have mathematical properties ideal for robust

79   parameter-fitting (Truccolo et al. 2005; Paninski et al. 2007).

80   For each recorded unit (median 69,672 frames and 550 spikes per unit), we computed the

81   GLM parameters that best predicted the unit's spike train given the whisker angle time series

82   using half the data as a training set for parameter-fitting; 8 total fitted parameters - 5 for

83   stimulus filter, 2 for history filter, 1 bias; Figure 2-figure supplement 3). We then assessed

84   prediction performance using the other half of the data as a testing set: we provided the GLM

85   with the whisker angle time series as input and calculated the predicted spike train, evoked in

86   response (Material and Methods). We then compared the recorded spike train to the GLM-

87   predicted one (Figure 2B-C) and quantified the similarity between the smoothed spike trains

88   using the Pearson correlation coefficient (PCC). This is a stringent, single-trial measure of

89   model prediction performance (Figure 2-figure supplement 1B). We then repeated this entire

90   procedure for the whisker curvature time series. Although angle GLMs predicted spike trains

91   of a few units moderately well (2/20 units had PCC > 0.5), they performed poorly for the

92   majority (median PCC 0.06, IQR 0.019-0.3; Figure 2B-D, orange). This was unlikely to be

93   because of non-linear tuning to whisker angle, since quadratic GLMs fared only marginally

94   better (median PCC 0.097, IQR 0.042-0.31; p=0.044, signed-rank test, Figure 2-figure

95   supplement 1A). In contrast, we found that, at the population level, the curvature GLMs were

96   substantially more accurate than the angle GLMs (median PCC 0.52, IQR 0.22-0.66;

97   p=0.0044, signed-rank test; Figure 2B-D, blue) with prediction accuracy up to PCC 0.88.

98   Curvature GLMs also predicted spikes during touch episodes significantly more accurately

99   (median PCC 0.57, IQR 0.23-0.72) than did angle GLMs during non-touch episodes (median

100   0.06, IQR 0.02-0.35; p=0.005, signed-rank test). At the level of individual units, 90% had

101   above chance PCC and we termed these 'curvature-sensitive' (Material and Methods). Of the

102   curvature-sensitive units, 61% were sensitive to positive curvature change and 39% to

103   negative curvature change (Material and Methods).

104   The result that curvature predicted PWN responses better than angle was robust to the

105   number of fitted parameters: a GLM sensitive to instantaneous curvature (4 parameters: 1

106   stimulus filter parameter, 2 history filter parameters and 1 bias) exhibited very similar

107   prediction accuracy (Figure 2-figure supplement 1C). The result was also robust to time-

108   scale: prediction accuracy based on curvature was significantly greater than that based on

109   angle for smoothing time-scales in the range 1-100ms (signed-rank test, $p<0.05$, Bonferroni-

110   corrected).

111   Although the activity of most units was better predicted by whisker curvature change than by

112   whisker angle, there was significant variability in prediction performance, and there were a

113   few units for which the angle prediction performance was appreciable (Figure 2D). However,

114   we found that this could largely be attributed to redundancy. When a mouse whisks against

115   an object, curvature change and angle fluctuate in concert (Birdwell et al. 2007; Bagdasarian

116   et al. 2013; Pammer et al. 2013; Figures 1E, 4E and Figure 4F-G). When we fitted GLMs

117   using both curvature change and angle as input, these GLMs predicted the spike trains no

118   more accurately (median PCC 0.53 IQR 0.40-0.62; $p=0.067$, signed-rank test; Figure 2D)

119   than GLMs based on curvature change alone. Moreover, on a unit-by-unit basis, for 65% of

120   units, curvature change GLMs predicted spikes better than angle (signed-rank test, $p<0.05$,

121   Bonferroni corrected); only for 5% of units did angle predict spikes better than curvature

122   change. GLMs based on curvature change also predicted spike trains more accurately than

123   GLMs based on "push angle" – the change in angle as the whisker pushes against an object

124   (Figure 1E; median PCC 0.25 IQR 0.04-0.45; $p=0.006$, signed-rank test). Moreover,

125   prediction accuracy of GLMs fitted with both push angle and curvature change (median PCC

126   0.52, IQR 0.2-0.69) inputs was no better than that of GLMs fitted with curvature alone (p =

127   0.43, signed-rank test)

128   In principle, neurons might also be sensitive to the axial force component (parallel to the

129   whisker follicle) and/or lateral force component (orthogonal to axial) associated with

130   whisker-object contact (Figure 1B-C, Figure 1-figure supplement 3; Solomon and Hartmann,

131   2006; Pammer et al. 2013). We restricted our analysis to bending moment since, under our

132   experimental conditions, axial/lateral force components were near-perfectly correlated with

133   bending moment (Figure 2-figure supplement 2) and bending moment is likely to have a

134   major influence on stresses in the follicle (Pammer et al.2013).

135   To further test the curvature-encoding concept, we asked whether curvature GLMs could

136   account for the response of PWNs to whisker-pole touch. To this end, we parsed the video

137   data into episodes of 'touch' and 'non-touch'. Units fired at a higher rate during touch than

138   otherwise (Szwed et al. 2003; Leiser and Moxon, 2007). Without any further parameter-

139   adjustment, the curvature-based GLMs reproduced this effect (Figure 2E): the correlation

140   coefficient between recorded and GLM-predicted firing rate for touch episodes was 0.97.

141   Collectively, the above results indicate that, during active touch, the best predictor of whisker

142   primary afferent firing is not whisker angle but rather the bending moment.

143

144   **Primary whisker neuronal activity during whisking is predicted by moment**

145   During free whisking - in the absence of whisker-pole contact - whisker curvature, and

146   therefore bending moment, changed little (Figure 1E, Figure 4F); consistent with previous

147   studies (Knutsen et al. 2008; Quist et al. 2014). Yet, 50% of recorded units ('whisking-

148   sensitive units') were significantly modulated by whisking amplitude (Figure 3A). Consistent

149   with Szwed et al. (2003), PWNs were diverse: 45% were curvature-sensitive (significant PCC

150   for curvature based GLM); 45% were both whisking and curvature sensitive and 5% were

151   whisking sensitive but not curvature-sensitive.

152   The presence of whisking sensitivity suggests that moment due to whisker bending is not the

153   only force that influences PWN activity. A likely candidate is the moment associated with the

154   rotational acceleration of a whisker: this moment is proportional to the whisker's angular

155   acceleration (Quist et al. 2014; Material and Methods). Consistent with this possibility, we

156   found that whisking-sensitive units were tuned to angular acceleration (Figure 3B) and that

157   50% of these were phase-modulated (Figure 3C). Angular acceleration tuning was diverse:

158   some units fired to acceleration in a particular direction (rostral or caudal), whilst others

159   responded to acceleration in both directions (Figure 3B, Figure 3-figure supplement 1).

160   Moreover, for whisking-sensitive units (but not whisking-insensitive ones), quadratic GLMs

161   trained on data from non-touch episodes were able to predict spikes using whisker angle

162   acceleration as input (Figure 3D-E; whisking sensitive units, median PCC 0.37, IQR 0.18-

163   0.58; non-whisking sensitive, median PCC -0.0071, IQR -0.035-0.041; p=0.0017 rank-sum

164   test for whisking-sensitive vs non whisking-sensitive units). For 70% of whisking-sensitive

165   units, directional selectivity for acceleration was consistent with that for curvature. These

166   findings indicate that, in the absence of whisker-object contact, responses of PWNs to

167   whisking itself can be accounted for by sensitivity to the moment associated with angular

168   whisker acceleration.

169

170   **Relation between kinematics and mechanics is different in active vs passive touch and**

171   **has implications for neural encoding**

172   We found, during active object exploration, that curvature change, but not whisker angle,

173   predicts PWN firing. In apparent contrast, studies using passive whisker stimulation have

174   reported that PWNs encode whisker angle and its temporal derivatives (Zucker and Welker,

175   1969; Gibson and Welker, 1983; Lichtenstein et al. 1990; Jones et al. 2004; Arabzadeh et al.

176   2005; Bale and Petersen, 2009; Lottem and Azouz, 2011; Bale et al. 2013). We wondered

177   whether the discrepancy might be due to differences in whisker mechanics between passive

178   and active stimulation conditions. To test this, we analysed the relationship between angle

179   and curvature change during active touch and compared it to that during passive whisker

180   stimulation. During active pole exploration, angle and curvature change were, over all, only

181   loosely related (median correlation coefficient 0.20, IQR 0.079-0.39, Figures 4D-E).

182   Important contributory factors were that the angle-curvature relationship was both different

183   for touch compared to non-touch (Figure 4F) and dependent on object location (Figure 4G).In

184   contrast, during passive stimulation, whisker angle was near perfectly correlated with

185   curvature change (for C2, correlation coefficients 0.96 and 0.94 respectively; similar results

186   for C5; Figures 4C-D, Figure 4E, inset and Figure 4-figure supplement 2); consistent with

187   properties of cantilevered beams (Birdwell et al. 2007). Simulations confirmed that, due to

188   the tight relationship between the variables, a unit tuned only to curvature change can appear

189   tightly tuned to angle (Figure 4-figure supplement 1). The implication is that apparent

190   sensitivity to whisker angle under passive stimulation conditions can be accounted for by

191   moment-tuning.

192

193   **DISCUSSION**

194   **Prediction of spikes fired by sensory neurons under natural conditions**

195 In the endeavour to understand how neurons encode and process sensory information, there is

196 a basic tension between the desire for tight experimental control and the desire to study

197 animals under natural, unconstrained conditions. Theories of sensory encoding suggest that

198 neural circuits have evolved to operate efficiently under natural conditions (Simoncelli and

199 Olshausen, 2001; Reinagel 2001). Previous studies have succeeded in predicting/decoding

200 spikes evoked by passive presentation of natural sensory stimuli to anaesthetised/immobilised

201 animals (Lewen et al. 2001; Arabzadeh et al. 2005; Pillow et al. 2008; Mante et al. 2008;

202 Lottem and Azouz, 2011; Bale et al. 2013), but it has been difficult to extend this approach to

203 encompass natural, active movement of the sense organs. Here we have addressed this

204 general issue, taking advantage of experimental possibilities recently created in the whisker

205 system (O'Connor et al.2010a), and the ability of computational methods, such as GLMs, to

206 uncover stimulus-response relationships even from data with complex statistical structure

207 (Paninski et al. 2007; Fairhall and Sompolinski, 2014). Our main finding was that responses

208 of PWNs, recorded as an awake mouse actively explores an object with its whiskers, can be

209 predicted from the forces acting on the whiskers. Given that, for each unit, we were

210 attempting to predict the entire ~70 s time course of activity, the variability of the behaviour

211 of untrained mice (O'Connor et al. 2010a), and the lack of trial-averaging as a noise

212 reduction strategy, it is remarkable that we found model prediction correlation coefficients up

213 to 0.88. A challenge of studying neural coding under unconstrained, awake conditions is that

214 sensory variables tend to correlate. A useful feature of the GLM training procedure is that it

215 takes such correlations into account. We found that, although whisker angle predicted spikes

216 for a subset of units, this effect was very largely explained by a curvature-coding model,

217 together with the correlation between angle and curvature.

218

219 **Mechanical framework for tactile coding**

220   Pushing a whisker against an object triggers spiking in many PWNs (Szwed et al. 2003,

221   2006; Leiser and Moxon, 2007). Biomechanical modelling by Hartmann and co-workers

222   accounts for this by a framework where the whisker is idealised as an elastic beam,

223   cantilever-mounted in the skin (Birdwell et al. 2007; Quist et al. 2014). When such a beam

224   pushes against an object, the beam bends, causing reaction forces at its base. Our data are in

225   striking agreement with the general suggestion that mechanoreceptor activity is closely

226   related to such reaction forces. Our results show that curvature change associated both with

227   contact-induced whisker bending and with whisker rotation predicts PWN spiking.   Our

228   results also provide a mechanical basis for previous findings: our finding of subtypes of

229   curvature-only and curvature-acceleration PWNs is consistent with previous reports of

230   'touch' and 'whisking-touch' units (Szwed et al. 2003; 2006).   Thus, a common framework

231   accounts for diverse PWN properties.

232   Our finding that whisker angle predicts PWN spikes poorly indicates that whisker angle can

233   change without modulating mechanotransduction in the follicle.   This is consistent with

234   evidence that, during artificial whisking, the follicle-shaft complex moves as a rigid unit

235   (Bagdasarian et al. 2013). In apparent contrast, previous studies using passive stimulation in

236   anaesthetised animals have consistently reported a tight relationship between whisker

237   kinematics and PWN response. In the cantilever whisker model, passively induced changes in

238   whisker angle correlate highly with whisker bending. We confirmed that this applies to real

239   whiskers *in vivo* and demonstrate that moment-sensitive units can thereby appear angle-

240   tuned. In this way, moment-encoding can account for primary neuron responses not only

241   during active touch but also under passive stimulation. More generally, our results highlight

242   the importance of studying neurons under natural, active sensing conditions.

243   In this study, we considered PWN encoding under conditions of pole contact, since this is

244   well-suited to reaction force estimation (O'Connor et al. 2010a; Pammer et al. 2013) and

11

245   involves object-stimulus interactions on a ~100 ms time-scale that is conducive to single-trial

246   analysis. Since whisker bending is ubiquitous in whisking behaviour, it is likely that our

247   finding of curvature sensitivity is a general one. However, prediction performance varied

248   across units, suggesting that other force components may also be encoded. Other

249   experimental conditions – for example, textured surfaces – may involve multiple force

250   components (Quist and Hartmann 2012; Pammer et al. 2013; Bagdasarian et al. 2013) and/or

251   encoding of information by spike timing on a finer time-scale (Panzeri et al. 2001; Petersen et

252   al. 2001; Arabzadeh et al. 2005; Bale et al. 2015).

253   It is axiomatic that mechanoreceptors are sensors of internal forces acting in the tissue within

254   which they are embedded (Abraira and Ginty, 2013) and therefore valuable to be able to

255   measure mechanical forces in the awake, behaving animal. In general, including the

256   important case of primate hand-use, the complex biomechanics of skin makes force-

257   estimation difficult (Phillips and Johnson, 1981). In contrast, for whiskers, the quasi-static

258   relationship is relatively simple: the bending moment on a whisker is proportional to its

259   curvature and this has the important implication that reaction forces can be directly estimated

260   from videography *in vivo* (Birdwell et al. 2007; O'Connor et al. 2010a; Pammer et al. 2013).

261   Our results are the first direct demonstration that such reaction forces drive primary sensory

262   neuron responses – likely involving Piezo2 ion channels (Woo et al. 2014; Poole et al.

263   2015;Whiteley et al. 2015) – and provide insight into how sensitivity to touch and self-

264   motion arises in the somatosensory pathway (Szwed et al. 2003; Yu et al. 2006; Curtis and

265   Kleinfeld, 2009; O'Connor et al. 2010b; Curtis and Kleinfeld, 2009; Huber et al. 2012;

266   Petreanu et al. 2012; Peron et al. 2015).

267   **Moment-based computations in tactile behaviour**

268 Extraction of bending moment is a useful first step for many tactile computations. Large

269 transients in bending moment signal object-touch events, and the magnitude of bending is

270 inversely proportional to the radial distance of contact along the whisker (Solomon and

271 Hartmann, 2006). As illustrated by our results on the statistics of active touch, if integrated

272 with cues for whisker self-motion, whisker bending can be a cue to the 3D location of an

273 object (Szwed et al. 2003, Szwed et al. 2006, Birdwell et al. 2007; Bagdasarian et al. 2013;

274 Pammer et al. 2013). Bending moment can permit wall following (Sofroniew et al. 2014) and,

275 if integrated across whiskers, can in principle be used both to infer object shape (Solomon

276 and Hartmann, 2006) and to map the spatial structure of the environment (Fox et al. 2012,

277 Pearson et al. 2013).

278 **Summary and Conclusion**

279 We have shown that the responses of primary whisker neurons can be predicted, during

280 natural behaviour that includes active motor control of the sense organ, from forces acting on

281 the whiskers. These results provide a bridge linking receptor mechanisms to behaviour.

282

13

283 **MATERIAL AND METHODS**

284 All experimental protocols were approved by both United Kingdom Home Office national

285 authorities and institutional ethical review.

286 **Surgical procedure**

287 Mice (C57; N=10; 6 weeks at time of implant) were anesthetized with isoflurane (2% by

288 volume in O_2), mounted in a stereotaxic apparatus (Narishige) and body temperature

289 maintained at 37°C using a homeothermic heating system. The skull was exposed and a

290 titanium head-bar (19.1mm x 3.2mm x 1.3mm; O'Connor et al. 2010a) was first attached to

291 the skull ~1 mm posterior to lambda (Vetbond), and then fixed in place with dental acrylic

292 (Lang dental). A craniotomy was made (+0.5mm to -1.5mm posterior to bregma, 0mm to

293 3mm lateral) and sealed with silicone elastomer. Buprenorphine (0.1 mg/kg) was injected

294 subcutaneously for postoperative analgesia and the mouse left to recover for at least 5 days

295

296 **Behavioural apparatus**

297 Mice were studied in a pole exploration apparatus adapted from O'Connor et al. (2010a) but

298 were not trained on any task. A mouse was placed inside a perspex tube (inner diameter 32

299 mm), from which its head emerged at one end, and immobilised by fixing the head-bar to a

300 custom mount holder. The whiskers were free of the tube at all times. The stimulus object

301 was a 1.59 mm diameter metal pole, located ~3.5mm lateral to the mouse's snout. To allow

302 control of its anterior/posterior location, the pole was mounted on a frictionless linear slide

303 (Schneeberger NDN 2-50.40) and coupled to a linear stepper motor (Zaber NA08B30). To

304 allow vertical movement of the pole into and out of range of the whiskers, the pole/actuator

305 assembly was mounted on a pneumatic linear slide (Festo SLS-10-30-P-A), powered by

306 compressed air. The airflow was controlled by a relay (Weidmüller). In this way, the pole

14

307   moved rapidly (~0.15 s) into and out of range of the whiskers. The apparatus was controlled

308   from Matlab via a real-time processor (TDT, RX8).

309   **Electrophysiology**

310   We recorded the activity of PWNs from awake mice in the following way. To permit reliable

311   whisker tracking (see below), before each recording session, A, B and E whisker rows were

312   trimmed to the level of the fur, under brief isoflurane anaesthesia. The trigeminal ganglion

313   was targeted as previously described (Bale et al. 2015). The silicone seal was removed and a

314   3/4 shank tungsten microelectrode array (FHC, recording electrodes 8MΩ at 1kHz, reference

315   1MΩ; tip spacing ~500 μm) was lowered through the brain (angle 4 ° to vertical in the

316   coronal plane) using a micromanipulator (Scientifica, PatchStar) under isoflurane

317   anaesthesia. Extracellular potentials were pre-amplified, digitised (24.4 kHz), filtered (band

318   pass 300-3000 Hz) and acquired continuously to hard disk (TDT, RZ5). The trigeminal

319   ganglion was encountered 6-7 mm vertically below the pial surface and whisker-response

320   units identified by manual deflection of the whiskers with a small probe. Once a well-isolated

321   unit was found, the whisker that it innervated (the 'principal whisker', PW) was identified by

322   manual stimulation. To define the PW, we deflected not only untrimmed whiskers but also

323   the stubs of the trimmed whiskers.   Any unit whose PW was a trimmed whisker was ignored.

324   At this point, anaesthesia was discontinued. Once the mouse was awake, we recorded

325   neuronal activity during repeated presentations of the pole ('trials'). Before the start of each

326   trial, the pole was in the down position, out of reach of the whiskers. The pole was first

327   moved anterior-posteriorly to a position chosen randomly out of a set of 11 possible

328   positions, spanning a range ±6 mm with respect to the resting position of the base of the PW.

329   A trial was initiated by activating the pneumatic slide relay, thus moving the pole up into the

330   whisker field, where it remained for 3s before being lowered. At the end of a recording

15

331 session, the microelectrode array was withdrawn, the craniotomy sealed with silicone

332 elastomer, and the mouse returned to its home cage.

High-speed videography

334 Using the method of O'Connor et al. (2010a) to image whisker movement/shape, whiskers

335 ipsilateral to the recorded ganglion were illuminated from below using a high-power infrared

336 LED array (940 nm; Roithner, LED 940-66-60) via a diffuser and condensing lens. The

337 whiskers were imaged through a telecentric lens (Edmunds Optics, 55-349) mounted on a

338 high speed camera (Mikrotron, LTR2; 1000 frames/s, 0.4 ms exposure time). The field of

339 view of the whiskers was 350x350 pixels, with pixel width 0.057mm.

Response to touch and non-touch events

341 Mouse whisking behaviour during the awake recording was segmented into 'touch', and 'non-

342 touch' episodes. Touches between the PW of each unit and the pole were detected manually

343 in each frame of the high-speed video. A frame was scored as touch if no background pixels

344 were visible between the pole silhouette and the whisker. Any frame not scored as a touch

345 was scored as non-touch. Touch and non-touch firing rates for a given unit were computed by

346 averaging activity over all corresponding episodes.

Whisker tracking

348 Since the trigeminal ganglion lacks topography, it is difficult to target units that innervate a

349 specific whisker, and therefore desirable for a whisker tracker to be robust to the presence of

350 multiple rows of whiskers. However, since neurons in the ganglion innervate individual

351 whiskers, it is sufficient to track only one whisker (the PW) for each recorded neuron. To

352 extract kinematic/mechanical whisker information, we therefore developed a whisker tracker

353 ('WhiskerMan'; Bale et al. 2015) whose design criteria, different to those of other trackers

354 (Perkon et al. 2011; Clack et al. 2012), were to: (1) be robust to whisker cross-over events;

16

355 (2) track a single, target whisker; (3) track the proximal segment of the whisker shaft. The

356 shape of the target whisker segment was described by a quadratic Bezier curve $\mathbf{r}(t,s)$ (a good

357 approximation away from the zone of whisker-object contact; Quist and Hartmann, 2012;

358 Pammer et al. 2013): $\mathbf{r}(t,s) = [x(t,s), y(t,s)]$, where x, y are horizontal/vertical coordinates of

359 the image, $s = [0,..,1]$ parameterises (x,y) location along the curve and t is time. We fitted

360 such a Bezier curve to the target whisker in each image frame using a local, gradient-based

361 search. The initial conditions for the search were determined by extrapolating the solution

362 curves from the previous two frames, assuming locally constant, angular velocity. The

363 combination of the low-parameter whisker description and the targeted, local search makes

364 the algorithm robust to whisker cross-over events. The 'base' of the target whisker was

365 defined as the intersection between the extrapolated Bezier curve and the snout contour

366 (estimated as described in Bale et al. 2015). The solution curve in each frame was visually

367 checked and the curves manually adjusted to correct occasional errors.

Estimation of kinematic/force parameters

369 The whisker angle (θ) in each frame was measured as the angle between the tangent to the

370 whisker curve at the base and the anterior-posterior axis (Figure 1B). Whisker curvature (κ)

371 was measured at the base as $\kappa = \frac{x'y'' - x''y'}{(x'^2 + y'^2)^{3/2}}$, where x', y' and x'', y'' are the first and second

372 partial derivatives of the functions $x(s)$ and $y(s)$ with respect to s (Figure 1B). Since reaction

373 force at the whisker base reflects changes in whisker curvature, rather than the intrinsic

374 (unforced) curvature (Birdwell et al. 2007), we computed 'curvature change' $\Delta\kappa = \kappa - \kappa_{int}$,

375 where κ_{int}, the intrinsic curvature, was estimated as the average of κ in the first 100 ms of the

376 trial (before pole contact; O'Connor et al. 2010a). During free whisking, whisker angle

377 oscillated with the characteristic whisking rhythm, but curvature changed little. The small

378 changes in whisker curvature during free whisking were consistent with torsional effects

17

379   (Knutsen et al. 2008). We estimated the number of whisking cycles from the duration of

380   touch/non-touch episodes and the whisking frequency: median 419 whisking cycles per unit

381   during touch periods; 415 during non-touch periods.

382   Under conditions of whisking against a smooth surface, such as in the present study, the

383   quasi-static framework of Birdwell et al. (2007) applies. Δκ, measured, at the base of a

384   whisker, in horizontal given plane, is proportional to the component of bending moment in

385   that plane. We used Δκ as a proxy for bending moment. Bending moment (M), Axial ($\vec{F}_{ax}$)

386   and lateral forces ($\vec{F}_{lat}$) at the whisker base were calculated, during periods of whisker-pole

387   contact, using the method of Pammer et al. (2013), using published data on areal moment of

388   inertia of mouse whiskers (Quist and Hartmann, 2012), along with whisker-pole contact

389   location (see figure 1-figure supplement 3 for details). Pole location, in the horizontal plane,

390   in each frame, was identified as the peak of a 2D convolution between the video image and a

391   circular pole template. To localise whisker-pole contact, the whisker tracker was used to fit

392   the distal segment of the whisker close to the pole, seeded by extrapolation from the whisker

393   tracking solution for the proximal whisker segment, described above. Whisker-pole contact

394   location was defined as the point where this distal curve segment was closest to the detected

395   pole centre. Pole and contact locations were verified by visual inspection.

396   As expressed by Newton's second law of rotational motion, the moment – or torque – of a

397   rigid body, rotating in a plane, is proportional to the body's angular acceleration. During free

398   whisking, a whisker behaves approximately as a rigid body and, for the whiskers considered

399   in this study, their motion is predominantly in the horizontal plane (Bermejo et al. 2002,

400   Knutsen et al. 2008). Thus, to assess whether such a moment is encoded by PWNs, we

401   measured angular whisker acceleration during free whisking as a proxy. Acceleration was

18

402   calculated from the whisker angle time series after smoothing with a Savitzky-Golay filter

403   (polynomial order 5; frame size 31 ms).

404   Push angle – the change in angle as a whisker pushes against an object - was measured during

405   touch epochs. For each touch episode, we determined the value of the angle in the frame

406   before touch onset and subtracted this from the whisker angles during the touch.

Passive whisker deflection

408   To determine how whiskers move/bend in response to passive deflection under anaesthesia, a

409   mouse was anesthetized (isoflurane 2%) and placed in the head-fixation apparatus. Individual

410   whiskers (C2 and C5 trimmed to 5 mm) were mechanically deflected using a piezoelectric

411   actuator as previously described (Bale et al. 2013; Bale et al. 2015). All other whiskers were

412   trimmed to the level of the fur. Each whisker, in turn, was inserted into a snugly fitting plastic

413   tube attached to the actuator, such that the whisker entered the tube 2 mm from the face. Two

414   stimuli were generated via a real-time processor (TDT, RX8): (1) a 10 Hz trapezoidal wave

415   (duration 3 s, amplitude 8°); (2) Gaussian white noise (duration 3 s, smoothed by convolution

416   with a decaying exponential: time constant 10 ms; amplitude SD 2.1 °). During the

417   stimulation, the whiskers were imaged as detailed above (1000 frames/s, 0.2 ms exposure

418   time).

Electrophysiological data analysis

420   *Spike sorting*: Single units (N=20) were isolated from the extracellular recordings as

421   previously described, by thresholding and clustering in the space of 3-5 principal components

422   using a mixture model (Bale and Petersen, 2009). A putative unit was only accepted if (1) its

423   inter-spike interval histogram exhibited a clear absolute refractory period and (2) its

424   waveform shape was consistent between the anaesthetised and awake phases of the recording.

425   *Responses to whisking without touch:* To test whether a unit responded to whisking itself, we

426   extracted non-touch episodes as detailed above and computed time series of whisking

427   amplitude and phase by band-pass filtering the whisker angle time series (6-30Hz) and

428   computing the Hilbert transform (Kleinfeld and Deschênes 2011). Amplitudes were

429   discretised (30 equi-populated bins) and the spiking data used to compute amplitude tuning

430   functions. Phases for bins where the amplitude exceeded a given threshold were discretised (8

431   equi-populated bins) and used to construct phase tuning functions. To determine whether a

432   unit was significantly amplitude-tuned, we fitted a regression line to its amplitude tuning

433   curve and tested whether the slope was statistically significantly different to 0 ($p=0.0025$,

434   Bonferroni corrected). To determine whether a unit was significantly phase-tuned, we

435   computed the maximum value of its phase tuning curve and compared this to the distribution

436   of maxima of chance tuning functions. Chance tuning functions were obtained by randomly

437   shifting the recorded spike sequences by 3000-8000 ms and recomputing tuning functions

438   (500 times). A unit was considered phase-tuned if its tuning function maximum (computed

439   using amplitude threshold of 2°) exceeded the 95th percentile of the shuffled distribution.

440   Acceleration tuning curves were quantified, for each unit, as follows. First, an acceleration

441   tuning curve was estimated (as above). Units typically responded to both positive and

442   negative accelerations, but with unequal weighting between them. To capture this, we fitted

443   the following regression model to the tuning curve:

$$r_i = \mu_0 + \mu_1|a_i| + \mu_2\Delta_i + \mu_3\Delta_i|a_i|$$

444   Here, for each bin i of the tuning curve, r_i was the firing rate and a_i was the acceleration; μ_0

445   μ_1, μ_2 and μ_3 were regression coefficients; the term Δ_i ($\Delta_i=1$ if $a_i<0$, $\Delta_i=0$ otherwise) allowed

446   for asymmetric responses to negative and positive acceleration. Based on its best-fitting

447   regression coefficients ($p=0.05$), units were classified as: having 'preference for negative

448   acceleration', if μ_3 was significantly >0; having 'preference for positive acceleration', if μ_3

449   was significantly <0; as having 'no preferred direction' if both μ_1 was significantly >0, and

450   μ_3 was not significantly >0; and as 'not acceleration sensitive' if neither μ_1 nor μ_3 were

451   significantly >0.

452   *Generalised Linear Model (GLM):* To investigate how well PWNs encode a given sensory

453   variable (e.g., whisker angle, curvature), we fitted single unit activity to a GLM (Nelder and

454   Wedderburn, 1972; Truccolo et al. 2005; Paninski et al. 2007), using methods similar to Bale

455   et al. (2013). For each unit, a 'stimulus' time series (*x*) (whisker angle or whisker curvature

456   change) and a simultaneously recorded spike time series (*n*) were discretized into 1 ms bins:

457   x_t and n_t denote respectively the stimulus value and spike count (0 or 1) in bin t.

458   GLMs express how the expected spike count of a unit depends both on the recent stimulus

459   history and on the unit's recent spiking history. The standard functional form of the model we

460   used was:

461     $$y_t = f\left(\vec{k}^T \vec{x_t} + \vec{h}^T \vec{n^*_t} + b\right), \qquad (1)$$

462   Here n^*_t, the output in bin t, was a Bernoulli (spike or no-spike) random variable. The

463   probability of a spike in bin t, y_t, depended on three terms: (1) the dot product between the

464   stimulus history vector $\vec{x_t} = (x_{t-Lk+1}, ..., x_t)$ and a 'stimulus filter' $\vec{k}$ (length $L_k = 5$); (2) the dot

465   product between the spike history vector $\vec{n}^* = (n^*_{t-Lh+1}, ..., n^*_t)$ and a 'spike history filter' $\vec{h}_t$

466   (length $L_h = 2$); (3) a constant b, which set the spontaneous firing rate. $f(\cdot)$ was the logistic

467   function $f(z) = (1 + e^{-z})^{-1}$. The preferred direction of the GLM is determined by the sign

468   of the stimulus filter. Positive (negative) k coefficients tend to make positive (negative)

469   stimuli trigger spikes. Since we found that GLM performance was just as good with $L_k = 1$ as

470     $L_k = 5$ (Figure 2-figure supplement 1C), we used results from the $L_k = 1$ case to define

21

471 selectivity to curvature change direction: positive k implies selectivity for positive curvature

472 change; negative k selectivity for negative curvature change. When a whisker pushes against

473 an object during protraction, curvature increases; when it pushes against an object during

474 retraction, it decreases.

475 To consider whether units might encode multiple sensory variables (e.g., both whisker angle

476 and whisker curvature change), we used a GLM with multiple stimulus history terms, one for

477 each sensory variable:

$$y_t = f\left(\vec{k}_1^T \overrightarrow{x_{t;1}} + \vec{k}_2^T \overrightarrow{x_{t;2}} + \vec{h}_t^T \overrightarrow{n^*} + b\right)$$

478 Here the indices 1, 2 label the sensory variables.

479 Training and testing of the GLM was done using a cross-validation procedure. For each unit,

480 half of the trials were assigned randomly to a training set and half to a testing set. The

481 training set was used to fit the parameters ($\vec{k}$, $\vec{h}$ and b), while the testing set was used to

482 quantify the similarity between the spike train of the recorded unit and that predicted by the

483 GLM. GLM fitting was achieved by finding the parameter values ($\vec{k}$, $\vec{h}$ and b), which

484 minimized a cost function consisting of the sum of the negative log-likelihood and a

485 regularizing term $-\propto \left\|\vec{k}\right\|^2$. For all units, model prediction performance on the test set was

486 robust to variation of α over several orders of magnitude: α was therefore set to a standard

487 value of 0.01. To quantify the performance of the model, the sensory time series of the testing

488 set was used as input to the best-fitting GLM to generate a 'predicted' spike train in response.

489 Both real and predicted spike trains were then smoothed by convolution with a 100 ms box-

490 car filter and the similarity between them quantified by the Pearson correlation coefficient

491 (PCC). For each unit, the entire training/testing procedure was repeated for 10 random

492 choices of training/testing set and the final prediction accuracy defined as the median of the

22

493   10 resulting PCC values. Data from these 10 samples were also used to test whether an

494   individual unit exhibited statistically significant prediction performance for different sensory

495   features. To test whether the results were robust to the smoothing time-scale, the above

496   procedure was repeated for a range of box-car smoothing filters (1, 5, 10, 20, 50, 70 ms). To

497   test whether a given 'actual' PCC was statistically significant, we tested the null hypothesis

498   that it could be explained by random firing at the same time-averaged rate as that of the

499   recorded unit. To this end, the recorded spike sequences were randomly shifted by 3000-8000

500   ms and the training/testing procedure above applied to this surrogate data. This was repeated

501   10 times and the resulting chance PCCs compared to the actual PCC using a signed-rank test,

502   p=0.0025 (Bonferroni corrected). This analysis was used to classify units as being 'curvature-

503   sensitive'.

504   *Quadratic GLM:* To test whether the units might exhibit nonlinear dependence on the

505   stimulus parameters, we adapted the GLM defined above (equation 1) to include quadratic

506   stimulus variables (Rajan et al. 2013). This was important to assess whisker angular

507   acceleration during free whisking, since a subset of units exhibited U-shaped acceleration

508   tuning functions (Figure 3B). Given a stimulus time series x_t, the quadratic stimulus history

509   vector was $[x_{t-Lk+1},...,x_t,x^2_{t-Lk+1},...,x^2_t]$. Fitting methods were otherwise identical to those

510   detailed above.

511   *Effect of angle-curvature correlations on apparent neuronal stimulus encoding in the passive*

512   *stimulation protocol:* If, in a given recording, sensory variable X correlates with sensory

513   variable Y, a neuron responsive purely to X will tend to appear tuned to Y. To investigate

514   whether such an effect might produce apparent sensitivity to whisker angle in the passive

515   stimulation paradigm, we simulated the response of curvature-tuned neurons to the whisker

516   curvature change time series measured during passive white noise stimulation. To minimise

517   free parameters, constrained GLMs (4 free parameters) were used, sensitive either to

518   instantaneous curvature ($\vec{k} = [\gamma]$) or to its first order derivative ($\vec{k} = \gamma$ [-1 1]), where γ was a

519   signed, gain parameter. Parameters ($\vec{h}$, b, γ) were adjusted to produce two spike trains (one

520   for training, the other for testing) with a realistic white noise induced firing rate (~50

521   spikes/s; Bale et al. 2013) . We then attempted to predict the simulated, curvature-evoked

522   (training) spike train by fitting GLMs (length 5 stimulus filter, 8 free parameters) using as

523   input either angle or curvature change. Cross-validated model accuracy was computed as the

524   PCC between the predicted spike train and the testing spike train (both smoothed by

525   convolution with a 5 ms box-car).

526   *Effect of single-trial approach on GLM prediction performance:* The objective of encoding

527   models, such as GLMs, is to obtain an accurate description of the mapping between a

528   stimulus and the neuronal spike trains it evokes. Since the random component of a neuron's

529   response is inherently unpredictable, the best any model can do is to predict the probability of

530   the spike train. To enable this, encoding models have generally (with few exceptions; Park et

531   al. 2014) been applied to a 'repeated-trials' paradigm, where a stimulus sequence (e.g., frozen

532   white noise) is repeated on multiple 'trials' (Arabzadeh et al. 2005; Lottem and Azouz, 2011;

533   Bale et al. 2013; Petersen et al. 2008; Pillow et al. 2008). Model accuracy can then be

534   quantified, largely free of contamination from random response variability, by comparing

535   (using PCC or otherwise) the trial-averaged response of the model to the trial-averaged

536   response of the neuron.

537   In contrast, in the present study of awake, actively whisking mice, the precise stimulus (time

538   series of whisker angle/curvature) was inevitably different on every pole presentation: there

539   were no precisely repeated trials to average over. Our standard model performance metric

540   (PCC) was computed by comparing the response on a single long, concatenated 'trial' the

541   corresponding GLM predicted response. Such a PCC is downwards biased by random

542   response variability.

543   To gauge the approximate magnitude of this downward bias, we used a simulation approach.

544   By simulating the response of model neurons, we could deliver identical, repeated trials and,

545   thereby compare model prediction performance by a metric based on trial-averaging with that

546   based on the single-trial approach. To this end, for each recorded unit, we used the best-

547   fitting curvature change GLM to generate 100 trials of spike trains evoked by the curvature

548   time series measured for that unit. Data from the first of these trials was used to fit the

549   parameters of a minimal 'refitted GLM' (stimulus filter length 1, spike history filter length 2;

550   bias; total 4 free parameters), and the single-trial performance quantified, using the approach

551   of the main text (Figure 2-figure supplement 1B, left). Next, we used the refitted GLM to

552   generate 100 repeated trials of spike trains evoked by the curvature time series. Repeated-

553   trials performance was then quantified as the PCC between PSTHs obtained by trial-

554   averaging (Figure 2, -figure supplement 1B, right).

25

559

560 **AUTHOR CONTRIBUTIONS**:

561 DC and RSP designed the study. DC and AE performed the experiments. DC, MHE and RSP

562 analyzed the data.MRB, AE, DC and RSP developed the experimental methods. DC, MHE

563 and RSP wrote the manuscript, with input from all authors.

564

565 **CONFLICT OF INTERESTS:**

566 The authors declare no competing financial interests.

567

REFERENCES

Abraira VE and Ginty DD. 2013. The sensory neurons of touch. *Neuron,* **79**: 618-639. doi:10.1016/j.neuron.2013.07.051

Arabzadeh E, Zorzin E and Diamond ME. 2005. Neuronal encoding of texture in the whisker sensory pathway. *PLoSBiol,* **3**:e17.doi: 10.1371/journal.pbio.0030017

Bagdasarian K, Swed M., Knutsen PM, Deutsch D, Derdikman D, Pietr M, Simony E. and Ahissar E. 2013. Pre-neuronal morphological processing of object location by individual whiskers. *Nat Neurosci*, **16**:622-631. doi:10.1038/nn.3378

Bale MR and Petersen RS. 2009. Transformation in the neural code for whisker deflection direction along the lemniscal pathway. *J Neurophysiol,* **102**:2771-2780. doi: 10.1152/jn.00636.2009

Bale MR, Campagner D, Erskine A and Petersen RS. 2015. Microsecond-Scale Timing Precision in Rodent Trigeminal Primary Afferents, *J Neurosci,* **35**: 5935-5940. doi: 10.1523/JNEUROSCI.3876-14.2015

Bale MR, Davies K, Freeman OJ, Ince RA and Petersen RS. 2013. Low-dimensional sensory feature representation by trigeminal primary afferents. *J Neurosci,* **33**: 12003-12012. doi: 10.1523/JNEUROSCI.0925-13.2013

Bermejo R, Vyas A, and Zeigler HP. 2002. Topography of rodent whisking-I. Two-dimensional monitoring of whisker movements. *Somatosens Mot Res*, **19(4)**: 341-346.doi: 10.1080/0899022021000037809

588 Birdwell JA, Solomon JH, Thajchayapong M, Taylor, MA, Cheely M, Towal RB, Conradt J

589 and Hartmann MJZ. 2007. Biomechanical models for radial distance determination by the rat

590 vibrissal system. *J Neurophysiol,* **98**:2439–2455. doi: 10.1152/jn.00707.2006

591 Clack NG, O'Connor DH, Huber D, Petreanu L, Hires A, Peron S, Svoboda K, Myers EW.

592 2012. Automated tracking of whiskers in videos of head fixed rodents. *PloS Comput Biol,*

593 **8**:e1002591. doi: 10.1371/journal.pcbi.1002591

594 Curtis JC and Kleinfeld D. 2009. Phase-to-rate transformations encode touch in cortical

595 neurons of a scanning sensorimotor system. *Nat   Neurosci,* **12(4)**: 492-

596 501.doi:10.1038/nn.2283

597 Diamond ME, von Heimendahl M, Knutsen PM, Kleinfeld D and Ahissar E. 2008. 'Where'

598 and 'what' in the whisker sensorimotor system. *Nat Rev Neurosci*, **9(8)**: 601-612.

599 doi:10.1038/nrn2411

600 Ebara S, Kumamoto K, Matsuura T, Mazurkiewicz JE and Rice FL. 2002. Similarities and

601 differences in the innervation of mystacial vibrissal follicle–sinus complexes in the rat and

602 cat: a confocal microscopic study. *J Comp Neurol*, **449(2)**, 103-119. doi: 10.1002/cne.10277

603 Fairhall A and Sompolisky H. 2014. Editorial overview: theoretical and computational

604 neuroscience. *Curr Opin Neurobiol,* **25**:1:236. doi:10.1016/j.conb.2014.02.010

605 Fox C, Evans M, Pearson M, and Prescott T. 2012. Tactile SLAM with a biomimetic

606 whiskered robot. In *IEEE International Conference on in robotics and automation (ICRA),*

607 4925-4930.

608 Gibson JJ. 1962. Observations on active touch. *Psychological Rev,* **69**: 477-491.

609 Gibson JM and Welker WI. 1983. Quantitative studies of stimulus coding in first-order

610 vibrissa afferents of rats. 1. Receptive field properties and threshold distributions. *Somatosens*

611 *Mot Res,* **1**:51-67. doi: 10.3109/07367228309144540

612 Hubel DH. 1959. Single unit activity in striate cortex of unrestrained cats. *J Physiol,***147.2**:

613 226-238. doi: 10.1113/jphysiol.1959.sp006238

614 Huber D, Gutnisky D, Peron S, O'Connor DH, Wiegert J. S., Tian L., Oertner T. G., Looger

615 L. L., and Svoboda K. 2012. Multiple dynamic representations in the motor cortex during

616 sensorimotor learning. *Nature,* **484:** 473-478. doi: 10.1038/nature11039

617 Jones LM, Depireux DA, Simons DJ and Keller A. 2004. Robust temporal coding in the

618 trigeminal system. *Science,* **304**: 1986-1989.doi: 10.1126/science.1097779

619 Khatri V, Bermejo R, Brumberg JC, Keller A and Zeigler HP. 2009. Whisking in air:

620 encoding of kinematics by trigeminal ganglion neurons in awake rats. *J Neurophysiol,* **101**:

621 1836-1846. doi: 10.1152/jn.90655.2008.

622 Kleinfeld D and Deschênes M. 2011. Neuronal basis for object location in the vibrissa

623 scanning sensorimotor system. *Neuron,* **72**:455-468. doi: 10.1016/j.neuron.2011.10.009.

624 Knutsen PM, Biess A and Ahissar E. 2008.Vibrissal kinematics in 3D: tight coupling of

625 azimuth, elevation, and torsion across different whisking modes. *Neuron,* **59**: 35-42.

626 Leiser SC and Moxon KA. 2007. Responses of trigeminal ganglion neurons during natural

627 whisking behaviors in the awake rat. *Neuron,* **53**: 117-133.doi:10.1016/j.neuron.2006.10.036.

628 Lettvin JY, Maturana HR, McCulloch WS and Pitts WH. 1959. What the frog's eye tells the

629 frog's brain. *Proc IRE,* **47**: 1940-1951.

630 Lewen GD, Bialek W, Steveninck RRDRV. Neural coding of naturalistic motion stimuli.

631 *Network,* **12(3)**: 317:329.

632 Lichtenstein SH, Carvell GE, and Simons DJ. 1990. Responses of rat trigeminal ganglion

633 neurons to movements of vibrissae in different directions. *Somatosens Mot Res,* **7**: 47-65.

634 doi: 10.1152/jn.90511.2008

635 Lottem E and Azouz R. 2011. A unifying framework underlying mechanotransduction in the

636 somatosensory system. *J Neurosci,* **31**: 8520-8532. doi: 10.1523/JNEUROSCI.6695-10.2011.

637 Mante V, Bonin V and Carandini M. Functional mechanisms shaping lateral geniculate

638 responses to artificial and natural stimuli. *Neuron,* **58**: 625-638. doi:

639 10.1016/j.neuron.2008.03.011

640 Nelder JA and Wedderburn RWM. 1972. Generalized linear models. *J R Statist SocSer A*,

641 **135**: 370–384.

642 O'Connor DH, Clack NG, Huber D, Komiyama T, Myers EW and Svoboda K. 2010a.

643 Vibrissa-based object localization in head-fixed mice. *J Neurosci,* **30**: 1947-1967. doi:

644 10.1523/JNEUROSCI.3762-09.2010.

645 O'Connor DH, Peron SP, Huber D and Svoboda K. 2010b. Neural activity in barrel cortex

646 underlying vibrissa-based object localization in mice. *Neuron*, **67**: 1048-1061. doi:

647 http://dx.doi.org/10.1016/j.neuron.2010.08.026.

648 Pammer L, O'Connor DH, Hires SA, Clack NG, Huber D, Myers EW and Svoboda K. 2013.

649 The mechanical variables underlying object localization along the axis of the whisker. *J*

650 *Neurosci*, **33**: 6726-6741. doi:10.1523/JNEUROSCI.4316-12.2013.

651   Paninski L, Pillow J and Lewi J. 2007. Statistical models for neural encoding, decoding, and

652   optimal stimulus design. *Prog Brain Res*, **165**: 493-507.doi:10.1016/S0079-6123(06)65031-0

653   Panzeri S, Petersen RS, Schultz SR, Lebedev M and Diamond ME. 2001. The role of spike

654   timing in the coding of stimulus location in rat somatosensory cortex. *Neuron*, **29(3)**, 769-

655   777.doi: 10.1016/S0896-6273(01)00251-3

656   Park IM, Meister ML, Huk AC and Pillow JW. 2014. Encoding and decoding in parietal

657   cortex   during   sensorimotor   decision-making.   *Nat   Neurosci*,**17**:   1395-1403.   doi:

658   doi:10.1038/nn.3800

659   Pearson MJ, Fox C, Sullivan JC, Prescott TJ, Pipe T and Mitchinson B. 2013. Simultaneous

660   localization and mapping on a multi-degree of freedom biomimetic whiskered robot. In *IEEE*

661   *International   Conference   on   robotics   and   automation   (ICRA)*,   586-592.doi:

662   10.1109/ICRA.2013.6630633

663   Perkon I, Košir A, Itskov PM, Tasič J and Diamond ME. 2011. Unsupervised quantification

664   of whisking and head movement in freely moving rodents. *J Neurophysiol,* **105:** 1950-

665   1962.doi: 10.1152/jn.00764.2010.

666   Peron SP, Freeman J, Iyer V, Guo C and Svoboda K. 2015.A Cellular Resolution Map of

667   Barrel   Cortex   Activity   during   Tactile   Behavior.   *Neuron,*   **86**:   783-799.   doi:

668   10.1016/j.neuron.2015.03.027

669   Petersen RS, Panzeri S, and Diamond ME. 2001. Population coding of stimulus location in

670   rat somatosensory cortex. *Neuron*, **32(3)**: 503-514.doi:10.1016/S0896-6273(01)00481-0

671   Petersen RS, Brambilla M, Bale MR, Alenda A, Panzeri S, Montemurro MA and Maravall

672   M. 2008. Diverse and temporally precise kinetic feature selectivity in the VPm thalamic

673   nucleus. *Neuron,* **60**: 890–903. doi: 10.1016/j.neuron.2008.09.041.

674   Petreanu L, Gutnisky D, Huber D, Xu N, O'Connor D, Tian L, Looger L and Svoboda K.

675   2012. Activity in motor-sensory projections reveals distributed coding in somatosensation.

676   *Nature,* **489**: 299-303. doi: 10.1038/nature11321.

677   Phillips JR and Johnson KO. 1981. Tactile spatial resolution. III. A continuum mechanics

678   model of skin predicting mechanoreceptor responses to bars, edges, and gratings. *J

679   Neurophysiol*, **46**: 1204-1225.

680   Pillow JW, Shlens J, Paninski L, Sher A, Litke AM, Chichilnisky EJ and Simoncelli EP.

681   2008. Spatio-temporal correlations and visual signalling in a complete neuronal population.

682   *Nature,* **454**: 995-999. doi: 10.1038/nature07140.

683   Poole K, Moroni M, and Lewin GR. 2015. Sensory mechanotransduction at membrane-

684   matrix interfaces. *Pflügers Archiv-European J Physiol*, **467**: 121-132. doi: 10.1007/s00424-

685   014-1563-6

686   Quist BW and Hartmann MJ. 2012. Mechanical signals at the base of a rat vibrissa: the effect

687   of intrinsic vibrissa curvature and implications for tactile exploration. *J Neurophysiol*, **107**:

688   2298–2312. doi: 10.1152/jn.00372.2011.

689   Quist BW, Seghete V, Huet LA, Murphey TD, & Hartmann MJ. 2014. Modelling forces and

690   moments at the base of a rat vibrissa during noncontact whisking and whisking against an

691   object. *J Neurosci*, **34(30)**: 9828-9844.

692   Rajan K, Marre O and Tkačik G. 2013. Learning quadratic receptive fields from neural

693   responses to natural stimuli. *Neural Comp*, **25**: 1661-1692. doi: 10.1162/NECO_a_00463.

694   Reinagel P. 2001. How do visual neurons respond in the real world? *Curr Opin Neurobiol*,

695   **11(4)**: 437-442. doi:10.1016/S0959-4388(00)00231-2

696   Rice FL, Mance A and Munger BL. 1986. A comparative light microscopic analysis of the

697   sensory innervation of the mystacial pad. I. Innervation of vibrissal follicle-sinus complexes.

698   *J CompNeurol*, **252(2)**: 154-174. doi: 10.1002/cne.902520203

699   Simoncelli EP and Olshausen BA.2001, Natural image statistics and neural representation,

700   *Ann Rev Neurosci*, **24**: 1193-1216. doi: 10.1146/annurev.neuro.24.1.1193.

701   Sofroniew NJ, Cohen JD, Lee AK, and Svoboda K. 2014. Natural whisker-guided behavior

702   by head-fixed mice in tactile virtual reality. *J Neurosci*, **34**: 9537-9550. doi:

703   10.1523/JNEUROSCI.0712-14.2014.

704   Solomon JH and Hartmann MJZ. 2006. Biomechanics: robotic whiskers used to sense

705   features. *Nature,* **443**: 525-525. doi: 10.1038/443525a.

706   Szwed M, Bagdasarian K and Ahissar E. 2003. Encoding of vibrissal active touch. *Neuron*,

707   **40**: 621–630. doi:10.1016/S0896-6273(03)00671-8.

708   Szwed M, Bagdasarian K, Bluenfeld B, Barak O, Derdikman D and Ahissar E. 2006.

709   Responses of trigeminal ganglion neurons to the radial distance of contact during active

710   vibrissal touch. *J Neurophysiol*, **95**: 791-802. doi: 10.1152/jn.00571.2005.

711   Truccolo W, Eden UT, Fellows MR, Donoghue JP and Brown EN. 2005. A point process

712   framework for relating neural spiking activity to spiking history, neural ensemble, and

713   extrinsic covariate effects. *J Neurophysiol,* **93**: 1074–1089. doi: 10.1152/jn.00697.2004.

714   Whiteley SJ, Knutsen PM, Matthews DW and Kleinfeld D. 2015. Deflection of a vibrissa

715   leads to a gradient of strain across mechanoreceptors in a mystacial follicle. *J Neurophysiol,*

716   **66**: 67. doi: 10.1152/jn.00179.2015.

717   Woo S-H et al. 2014. Piezo2 is required for Merkel-cell mechanotransduction. *Nature,* **509**:

718   622-626. doi:10.1038/nature13251.

719   Yarbus AL. 1967. Eye movements and vision. New York: Plenum Press.

720   Yu C, Derdikman D, Haidarliu S and Ahissar E. 2006. Parallel thalamic pathways for

721   whisking and touch signals in the rat. *PLoS Biol,***4**, e124. doi: 10.1371/journal.pbio.0040124

722   Zucker E and Welker WI. 1969. Coding of somatic sensory input by vibrissae neurons in the

723   rat's trigeminal ganglion. *Brain Res,* **12**: 138-156. doi:10.1016/0006-8993(69)90061-4

724 **Figure 1. Electrophysiological recording from single primary whisker units in awake,**

725 **head-fixed mice and simultaneous measurement of whisker kinematics/mechanics.**

726 **A.** Schematic of the preparation, showing a tungsten microelectrode array implanted into the

727 trigeminal ganglion of ahead-fixed mouse, whilst a metal pole is presented in one of a range

728 of locations (arrows). Before the start of each trial, the pole was moved to a randomly

729 selected, rostro-caudal location. During this time, the whiskers were out of range of the pole.

730 At the start of the trial, the pole was rapidly raised into the whisker field, leading to whisker-

731 pole touch. Whisker movement and whisker-pole interactions were filmed with a high-speed

732 camera.

733 **B and C.** Kinematic (whisker angle θ) and mechanical (whisker curvature κ, moment $\vec{M}$,

734 axial force $\vec{F}_{ax}$ and lateral force $\vec{F}_{lat}$) variables measured for the principal whisker in each

735 video frame. When a whisker pushes against an object during protraction (as in panel **D**, red

736 and cyan frames), curvature increases; when it pushes against an object during retraction (as

737 in panels and **C**), it decreases.

738 **D.** Individual video frames during free whisking (yellow and green) and whisker-pole touch

739 (red and cyan) with tracker solutions for the target whisker (the principal whisker for the

740 recorded unit, panel **E**) superimposed (coloured curve segments).

741 **E.** Time series of whisker angle push angle and curvature change, together with

742 simultaneously recorded spikes (black dots) and periods of whisker-pole contact (red bars).

743 Coloured dots indicate times of correspondingly coloured frames in **D**.

744

745

746

35

Figure 2. Primary whisker neurons encode whisker curvature, not whisker angle, during active sensation.

A. Schematic of the Generalized Linear Model (GLM).

B. For an example unit, whisker angle (top panel), whisker curvature change (middle panel) and simultaneously recorded spike train (bottom panel, black), together with predicted spike trains for the best-fitting angle GLM (bottom panel, orange) and curvature change GLM (bottom panel, blue). Spike trains discretized using 1 ms bins and smoothed with a 100 ms boxcar filter. Prediction performance (Pearson correlation coefficient, PCC) for this unit was 0.59. Inset shows tuning curves for both GLMs, computed by convolving the relevant sensory time series (angle or curvature change) with the corresponding GLM stimulus filter to produce a time series of filter coefficients, and estimating the spiking probability as a function of filter coefficient (25 bins).

C. Analogous to panel **B.** for a second example unit. Prediction performance PCC for this unit was 0.74.

D. Prediction performance between predicted and recorded spike trains) compared for GLMs fitted with three different types of input: curvature change alone; angle alone; both curvature change and angle. Each blue/orange/green dot is the corresponding PCC for one unit: large black dots indicate median; error bars denote inter-quartile range (IQR). To test statistical significance of each unit's PCC, the GLM fitting procedure was repeated 10 times on spike trains subjected each time to a random time shift: magenta dots show these chance PCCs for the unit indicated by the magenta circle; the mean chance PCC was computed for each unit and the large gray dot shows the median across units. Black circles indicate units whose PCC was significantly different to chance (signed-rank test, Bonferroni corrected, $p<0.0025$). To

770 facilitate direct comparison between results for curvature change GLM and angle GLM, these

771 are re-plotted in the inset.

772 **E. Left.** Firing rate during touch episodes compared to that during non-touch episodes for

773 each unit, compared to corresponding predicted firing rates from each unit's curvature change

774 GLM. **Right.** Medians across units: error bars denote IQR; * denotes differences significant

775 at p<0.05 (signed-rank test).

776 **Figure 3. Primary whisker neurons encode whisker angular acceleration during free**

777 **whisking**

778 **A.** Mean response of an example whisking-sensitive unit to whisking amplitude, computed

779 during non-contact episodes (dark green, shaded area shows SEM) with regression line

780 (black). Inset shows regression line slopes (median and IQR) for whisking sensitive (green)

781 and non-whisking sensitive (grey) units. * indicates statistically significant rank-sum test

782 (p=0.05).

783 **B.** Mean response of two example units as a function of angular acceleration. The dark brown

784 unit is the same as that shown in A.

785 **C.** Mean response of two example units as a function of whisking phase. The dark pink unit

786 is the same as that reported in A; the light pink unit is the same as that shown as light brown

787 in B.

788 **D.** Excerpt of free whisking **(orange)** along with activity of an example, whisking-sensitive

789 unit (black) and activity predicted by a GLM driven by angular acceleration (brown). The

790 unit is the same as that shown in **A**.

791 **E.** GLM prediction accuracy (PCC) for all whisking sensitive (brown) and whisking

792 insensitive units (grey). Bars and vertical lines denote median and IQR respectively.

793 **Figure 4. Whisker angle and whisker curvature change are highly correlated during**

794 **passive whisker deflection, but decoupled during active touch.**

795 **A.** Whisker angle (**top**) and whisker curvature change (**bottom**) time series, due to passive,

796 trapezoidal stimulation of C2 whisker in an anaesthetized mouse, estimated as mean over 10

797 repetitions. Note that error bars (showing SEM) are present but very small.

798 **B.** Corresponding data for low-pass filtered white noise (hereafter abbreviated to 'white

799 noise') stimulation of the same whisker.

800 **C.** Cross-correlation between curvature change and angle during white noise stimulation, for

801 C2 whisker.

802 **D.** Cross-correlation between angle and curvature change at zero lag, for both passive

803 stimulation under anaesthesia and awake, active sensing (median of absolute cross-

804 correlation for each unit; error bar denotes IQR).

805 **E.** Joint distribution of whisker angle and whisker curvature change in awake, behaving mice

806 (1 ms sampling). Different colours denote data corresponding to different recorded units.

807 **Inset**: Analogous plot for passive, white noise whisker deflection in an anaesthetised mouse.

808 Different colours indicate data from different whiskers.

809 **F.** Joint distribution of angle and curvature change for an example recording from an awake

810 behaving mouse, with samples registered during touch and non-touch distinguished by colour

811 (1 ms sampling).

812 **G.** Touch data of **F** classified according to pole position (dot colour).

813

814

815   **SUPPLEMENT**

816   **Figure 1-figure supplement 1. Electrophysiological recording from trigeminal primary**

817   **neurons of awake, head-fixed mice.**

818   Extracellular potential recorded from the same single unit during both anaesthetized and

819   awake epochs. Spikes belonging to the cluster of the target unit are shown by black triangles.

820   Inset shows overlay of all waveforms belonging to this cluster.

821

822   **Video 1: Video of an awake mouse, exploring a pole with its whiskers with simultaneous**

823   **electrophysiological recording of a primary whisker neuron**

824   At the start of the video, the pole is out of range of the whiskers. Whisker tracker solution for

825   the principal whisker of the recorded unit is overlaid in red. White dots represent spikes;

826   orange trace shows whisker angle (scale bar = 40 $^{\circ}$); blue trace shows whisker curvature

827   change (scale bar = 0.05 mm^{-1}). Video was captured at 1000 frames/s and is played back at

828   50 frames/s. Related to Figure 1.

829

830   **Figure 1- figure supplement 3. Computation of axial and lateral contact forces.**

831   Axial (F_{ax}) and lateral (F_{lat}) force components at the whisker base were calculated, in each

832   video frame where there were whisker-pole contacts, as follows (Pammer et al. 2013). First,

833   the point of whisker-pole contact was located (Experimental Procedures). The direction of

834   the force $\vec{F}$ was then calculated as the normal to the whisker tangent at the contact point

835   (Pammer et al. 2013). Moment at the base M was calculated from the whisker curvature at

836   the base (Material and Methods) and then the magnitude F of $\vec{F}$ was derived from the

837   definition of moment:

$$F = \frac{M}{r\sin(\varphi)}$$

838

839   where r is the magnitude of the lever arm vector $\vec{r}$ from whisker base to contact point, and φ

840   is the angle between $\vec{r}$ and $\vec{F}$. The components F_{ax} and F_{lat} were then found by projecting $\vec{F}$

841   onto the tangent and normal to the whisker at its base, respectively:

842    $F_{ax} = F\sin\left(\theta_{base} - \theta_{contact}\right),$

843    $F_{lat} = F\cos\left(\theta_{base} - \theta_{contact}\right).$

844   Here θ_{base} is the angle between the tangent to the whisker at its base and the horizontal;

845    $\theta_{contact}$ is the angle between $\vec{F}$ and the horizontal.

846

847

848

849

850

851

852

853

854

855 **Figure 2- figure supplement 1. Effect on GLM performance of quadratic input terms,**

856 **simulated repeated trials and minimal stimulus filters**

857 **A.** Angle GLM prediction performance is robust to addition of quadratic stimulus-

858 dependence. Prediction accuracy (PCC) for standard angle GLM (same data as Figure 2C of

859 main text) in comparison to quadratic GLM (see Material and Methods). Black dots denote

860 medians, error bars IQR.

861 **B.** Single-trial GLM prediction accuracy is limited by neuronal response variability.

862 Prediction accuracy (PCC) for simulated neurons. Each simulated neuron is the best-fitting

863 GLM, based on instantaneous curvature change, for its corresponding recorded unit (see

864 Material and Methods). Prediction accuracy is quantified both using the single-trial approach

865 of the main text and using a repeated-trial method only possible by virtue of using a

866 simulation. Black dots denote medians, error bars IQR.

867 **C.** Prediction accuracy of curvature-based GLMs is accounted for by tuning to instantaneous

868 curvature change.A GLM performs a temporal filtering operation on its sensory stimulus

869 input and the sensory feature(s) which it encodes is determined by this 'stimulus filter'. The

870 stimulus filters can, in principle, be complex, but we found that the ability of a GLM to

871 predict spikes (**lower left**) from curvature change was fully explained by the simple case

872 where the action of the stimulus filter is simply to multiply the sensory input by a gain factor

873 (median 0.55, IQR 0.26-0.66; p=0.35 signed-rank test).Recorded spike train (**upper left**) and

874 curvature-predicted spike trains (**lower left**) both for a 'curvature history' GLM with a length

875 5 stimulus filter identical to Figure 2D of main text and for an 'instantaneous curvature'

876 GLM with a length 1 stimulus filter. Data for unit 2 of main text Figure 2C. Prediction

877 accuracy of the curvature history GLM compared to that of the instantaneous curvature GLM

878 for every recorded unit (**right**).

41

879   **D.** Tuning curves for curvature change (blue) and angle (orange) of unit 1 and unit 2 in

880   Figure 2.

881

882   **Figure 2- figure supplement 2. Moment is near-perfectly correlated with axial/lateral**

883   **contact force components during pole exploration.**

884   **A.** Two example time series for simultaneously measured whisker angle, bending moment,

885   lateral force and axial force (see Material and Methods). Red bars indicate episodes of

886   whisker-pole contact.

887   **B.** Joint distribution of bending moment and lateral force (**left**), compared to that of bending

888   moment and axial force (**right**), for the same recording shown in **A**. Moment was highly

889   linearly correlated with lateral force (median absolute correlation coefficient across units

890   0.995, IQR 0.99-1.00, median R^2 of linear fit 0.99, IQR 0.97-1.00), and highly quadratically

891   correlated with axial force (median R^2 of quadratic fit 0.94, IQR 0.85-0.98). This indicates

892   that, during our conditions of pole exploration, axial force and lateral force are both

893   redundant with moment

894   **Figure 2- figure supplement 3. Example filters for curvature-based GLMs.**

895   Stimulus filter, history filter and bias term of curvature-based GLMs for two units (**A** and **B**),

896   fitted as described in Material and Methods. Both units had negative history filters (in the 2

897   ms preceding a spike), consistent with refractoriness. The stimulus filter of unit B was

898   negative (in the 5 ms preceding a spike), indicating sensitivity to negative curvature change.

899   The stimulus filter of unit A was biphasic, but with positive integral, indicating sensitivity

900   both to positive curvature change and to positive curvature change derivative. Under our

901   stimulus conditions, dominated by slow (~100 ms) time-scale whisker-pole interactions, the

902   former effect was dominant; derivative-sensitivity had relatively little impact on spike

903   prediction.

904

905   **Figure 3- figure supplement 1. Whisking-sensitive units exhibit heterogeneous**

906   **selectivity to angular acceleration.**

907   For each whisker-sensitive unit, an acceleration tuning curve was estimated (Figure 3B).

908   Tuning to positive (negative) acceleration was quantified by the slope of a regression line

909   fitted to the positive (negative) acceleration half of the tuning curve. In general, units

910   responded to both positive and negative accelerations but to different degrees. Statistical

911   tests, based on regression coefficients, detailed in Material and Methods, were used to

912   differentiate the different types of unit.

913 **Figure 4-figure supplement 1: Correlations between angle and curvature change during**

914 **passive whisker stimulation can make curvature-tuned units appear angle-tuned.**

915 The data of Figure 4 show a strong correlation between whisker angle and whisker curvature

916 during passive stimulation of the whisker. To test whether this correlation might make

917 curvature-tuned units appear angle-tuned, we used a simulation approach. This allowed us to

918 generate responses from idealised neurons whose true tuning was known, by construction, to

919 be only to curvature. We simulated responses of such neurons to the curvature change time

920 series obtained from passive white noise stimulation (**A1-2**). We then trained a GLM to

921 predict these curvature-evoked spikes using only whisker angle as input (**A3-A4**). Despite

922 being fed the 'wrong' input, this GLM was able to predict the spikes accurately (for C2

923 whisker, angle PCC was 0.90, curvature change PCC 0.94; results similar for C5; **C**). This

924 result was robust to different choices of feature tuning (**B-C**).

925 **A1.**Whisker curvature change caused by the white noise stimulus applied to C2 whisker of an

926 anaesthetized mouse (same data as main text Figure 3, repeated for clarity).

927 **A2.** Spike train evoked by a simulated curvature-tuned neuron in response to the stimulus in

928 A1 (a GLM with the position filter shown in left panel of A5).

929 **A3.**Whisker angle time series corresponding to panel A1.

930 **A4**. Target response (black) compared to predicted response from best-fitting GLMs using

931 either angle (orange) or curvature change (blue) as input.

932 **A5**. **Left**. Stimulus filter used to generate the spike train of panel A2. **Middle-Right**. Best-

933 fitting stimulus filters (normalised to unit length) for GLMs trained on the spikes of panel A2

934 and the angle time series of panel A3 or the curvature change time series of panel A1

935 respectively.

45

936   **B1-5**.Results analogous to A1-5 for a simulated neuron tuned to curvature velocity.

937   **C**. Quantification of the GLM predictions shown in panels A4-B4.
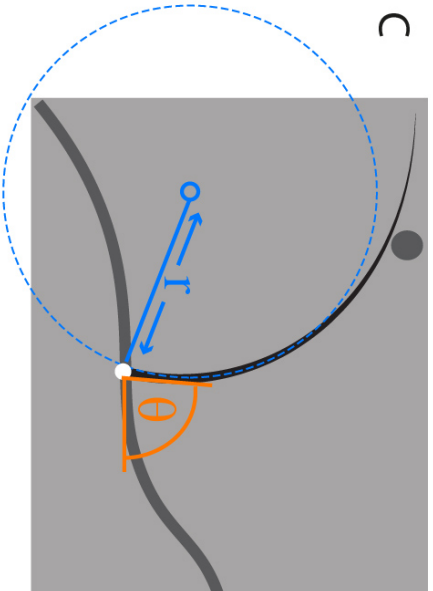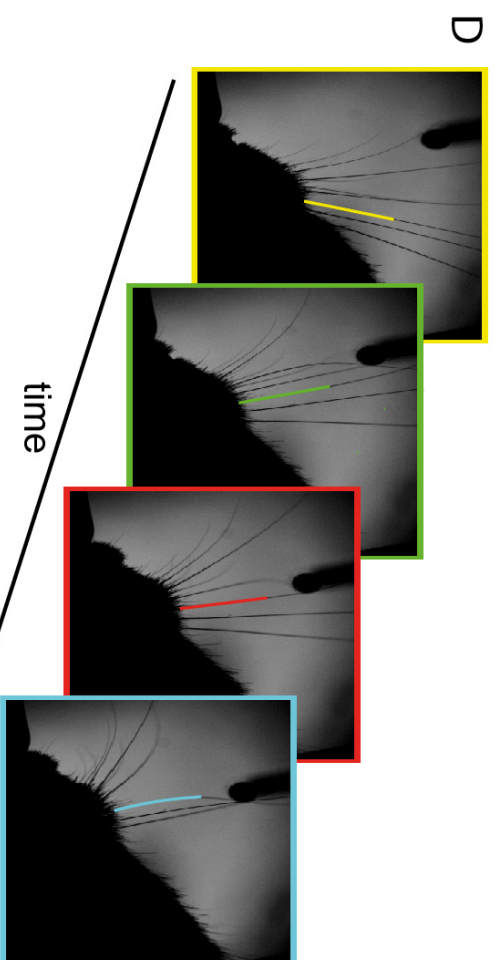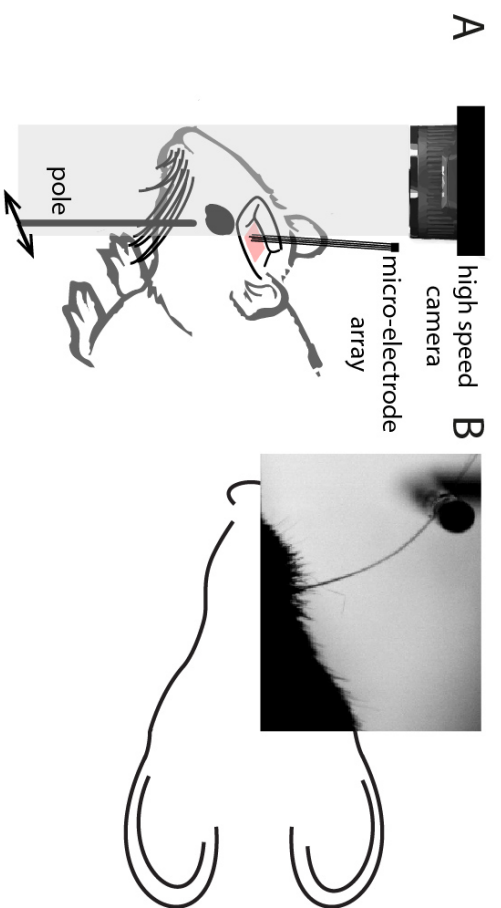
938

939   **Figure 4-figure supplement 2. Measurement of whisker bending during passive whisker**
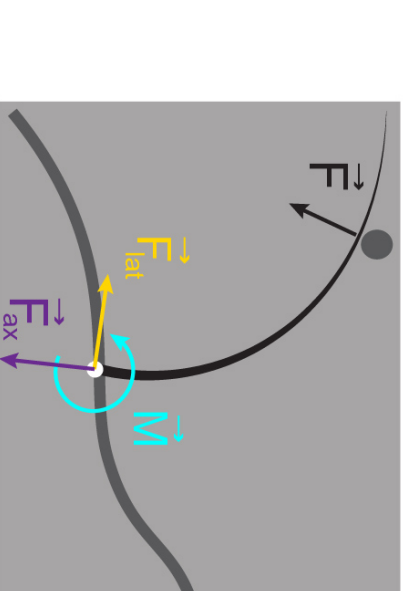
940   **deflection.**

941   **A.** Four video frames taken during trapezoidal, passive whisker stimulation with whisker tracker

942   solutions overlaid (coloured lines).

943   **B.** Curvature change (left) and corresponding tracker solutions (right) during a 45 ms episode.

944   Coloured dots mark the times of the example frames in panel A and shading from blue to aqua

945   indicates curvature change. This whisker has negative intrinsic curvature. As the actuator applies

946   force to the whisker, the whisker straightens up and the curvature increases.

947